Prediction of Swirl Effects on Fan-OGV Interaction Tones

Oluwaseun E. Adetifa*, Alan McAlpine†
Institute of Sound and Vibration Research, University of Southampton, SO17 1BJ, UK

Howoong Namgoong‡
Rolls-Royce plc., Derby, DE24 8BJ, UK

Noise levels predicted for the fan-OGV interaction tones generated by modern high and ultra high bypass ratio aircraft engines are significantly changed when swirl in the interstage region is included in the modelling. An analytical prediction method is used to predict interstage interaction tonal noise levels for an annular duct with uniform flow or swirling flow. It is predicted that swirl effects alter the range of modes that are cut-on, and their corresponding sound power levels in the upstream direction. Results confirm that the inclusion of swirl effects in the modelling of fan-OGV interaction tones is important to improve the prediction of the sound power levels of the upstream propagating modes.

Nomenclature

A = Duct area $\pi(r_d^2 - r_h^2)$

a_0 = speed of sound

b, $\tilde{b}$ = vane semi-chord, half of vane semi-chord/tip vane semi-chord

B = number of blades

This is the author's version (pre-print) of the work that was accepted for publication in the proceedings of the 28th AIAA/CEAS Aeroacoustics Conference held in Southampton, UK, June 14–17 2022.

The final version was published in the proceedings of the conference as paper No. 2022-2942.

https://doi.org/10.2514/6.2022-2942

*Research Fellow, ISVR, University of Southampton, UK, o.e.adetifa@soton.ac.uk
†Associate Professor, ISVR, University of Southampton, UK
‡Noise Engineer, Rolls-Royce, Derby, UK

c_1, c_2	=	blade chord, vane chord
CFD	=	Computational Fluid Dynamics calculations
f, f_q	=	vane loading, qth harmonic of f
h	=	hub-to-tip ratio
k	=	wavenumber
l	=	Lean distance at radius r
M, M_r	=	axial, relative, tangential Mach number
m, n	=	Azimuthal, radial orders
OGV	=	Outlet Guide Vanes
p, $\hat{p}$, P, P_w	=	acoustic pressure, complex pressure, modal pressure amplitude, sound power level
r, r_h, r_d	=	radial distance, hub radius, duct radius
s	=	Sweep distance at radius r
t	=	time
U,U_θ, U_r, v_n, v_q, $\check{v}_q$	=	axial, relative flow, upwash velocity, qth harmonic of v, nondimensional v_q
V	=	number of outlet guide vanes
y, Y	=	chord normal distance, non-dimensional chordwise normal
z, Z	=	axial distance, non-dimensional chordwise distance
α	=	stagger angle
β	=	$\sqrt{1 - M_r^2}$
γ, $\tilde{\gamma} = \gamma r_d$	=	axial wavenumber of duct mode in stator-fixed frame
κ	=	duct mode radial eigenvalue
ρ	=	fluid density
σ_c	=	tip vane chord/duct radius
θ	=	azimuthal distance/direction
ω, Ω	=	angular frequency, fan rotational speed

I. Introduction

The need to meet increasingly stringent aircraft noise regulations, and the development of new ultra-high bypass aircraft engines, demand reliable methods for noise prediction and control. To control the noise, the ability to adequately account for various noise mechanisms in the noise prediction is very important. Development of methods for the estimation of noise levels from various aircraft noise sources, and the improvement of existing methods, tools and technologies are on-going tasks in the aviation industry.

This article focusses on the prediction of the tones generated from the interaction of the fan wakes with the downstream outlet guide vanes (OGVs) or engine section stators (ESSs), which is one of the many aircraft engine noise sources. More specifically, the article examines the significance of having the effect of swirl incorporated in the prediction of fan-OGV interaction tones.

It is noted that various studies have been carried out on fan-OGV or rotor-stator interaction noise in past research activities over many decades. Among the notable works are those of Tyler and Sofrin [1], Ventres et al. [2], Meyer & Envia [3] among others. To predict interaction tones analytically or semi-analytically, methods which have been explored previously include those pertaining to the characterization of the wakes shed from airfoils and fans/rotors, response of the blade row to impinging vortical gusts/wake [4], and Green function models for annular ducts [2, 3].

The main advantage of analytical prediction methods is to be able to quickly determine changes in the predicted noise, and to carry out parametric/design sweeps at very low computational cost. An adequate rotor-stator interaction tone prediction for future aero-engine architectures using analytical and/or empirical methods must be suitable for the novel architectures of fans, stator vanes and engine ducts. Furthermore, such methods must be able to examine the effects of variation in rotor blade or stator vane count, and the axial gap between the fan blades and the stator vanes.

Presented in the article are the results from such a prediction method with particular focus on the comparison between the output modal sound levels for cases where the flow is regarded as uniform flow to those where the swirl effects have been included in the calculations. In the article, first the assumptions and simplifications of the modelling are discussed. In the subsequent sections, an overview of the method is presented. This includes modelling the fan wakes, upwash, cascade response and unsteady lift for stators. Additionally, duct acoustics theory is used to model the sound field in a rigid, hard-walled duct in terms of a tailored Green function constructed from Fourier–Bessel modes. The output of the prediction method is evaluation of the sound power in the cut-on modes propagating upstream and

downstream of the stator vanes. Outputs are thereafter compared for test cases and against representative fan rig engine test data.

II. Assumptions, idealization, geometry and coordinates

Employing methods that are mainly analytical or semi-analytical satisfy the requirements for a low-cost, low-fidelity prediction method. Two-dimensional theory for thin airfoils is the foundation for the analytical work. This approximation allows the velocity field downstream of the rotor to be used to represent the mean flow. Unsteady components which are convected to the leading edge plane of the downstream stators are used to evaluate the upwash velocity, while imposing the necessary boundary conditions on the interaction surfaces. A streamtube approach, where

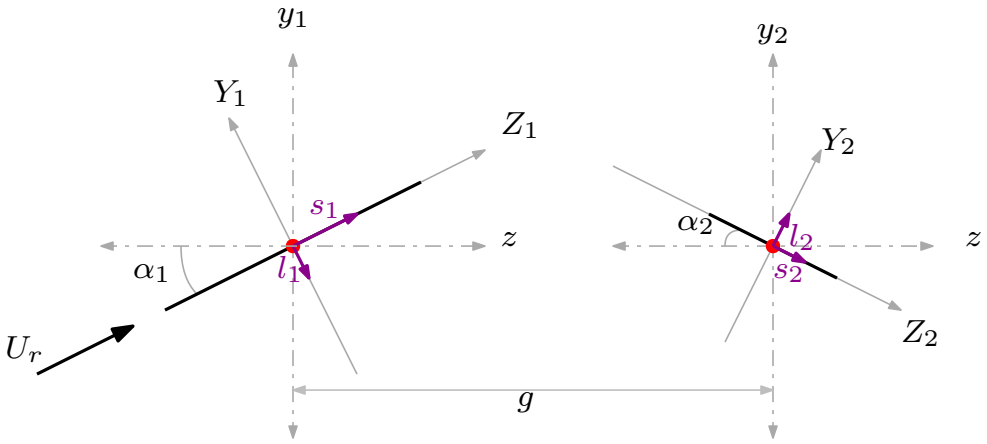

Fig. 1 Reference blade/vane coordinates with lean and sweep

the rotor, stator and duct space are regarded as annular strips and unwrapped at the radius that describes each strip, forms the basis for the stator response model. This gives a two-dimensional cascade of blades or vanes. A further simplification is that the blades and vanes are taken to have zero thickness (flat plates). Figure 1 shows a reference blade and vane, their respective local coordinates (y_1, z_1), (Y_1, Z_1) for the blade, and (y_2, z_2), (Y_2, Z_2) for the vane, with stagger angles α, sweep s, lean l, and axial gap g. All the blades are exactly alike and any perturbations in the flow in a strip are periodic and considered to be two-dimensional.

The acoustic perturbations in the subsonic uniform flow are considered to be small allowing the use of linear theory, and the effect of thickness and camber to be neglected with the plates assumed thin airfoils or flat plates [4]. Hence, these thin airfoils are set to operate at zero incidence. When uniform flow is considered, an inviscid flow assumption is made which eliminates the need to consider the boundary layer at the solid boundaries.

For rotor-stator predictions, the axial distance over which the wakes convect from the fan blades' trailing edges to the stator leading edge, the stagger angle of the stator vanes, the frequency of the wakes, and the angle of incidence of the mean flow are all important quantities. These influence the magnitude of the unsteady lift, and, hence, the response of the stator vanes, and, directly, the noise that is generated. Although the effect of the geometry of blades and vanes can significantly affect predictions depending on the operation conditions, the focus on analytical methods necessitates reasonable simplifications. Various previous studies [2, 3, 5] have shown that these simplifications provide useful and reliable predictions.

Using the annular strip approach allows variations in all geometric parameters with respect to the radius including the axial distance, blade/vane chord, sweep and lean. These are specified with respect to their values at the hub. Similarly, simplification of the duct geometry is carried out to enable analytical methods to be used. The duct is considered to be an annular duct where each strip is defined by a radius. The presence of the engine section stators (ESSs) and the outlet guide vanes (OGVs) is simplified, as shown in figure 2. This together with the strip approach allows that the different axial distances to the OGV and ESS and their radial spans can be carefully modelled. Additonally, this set up

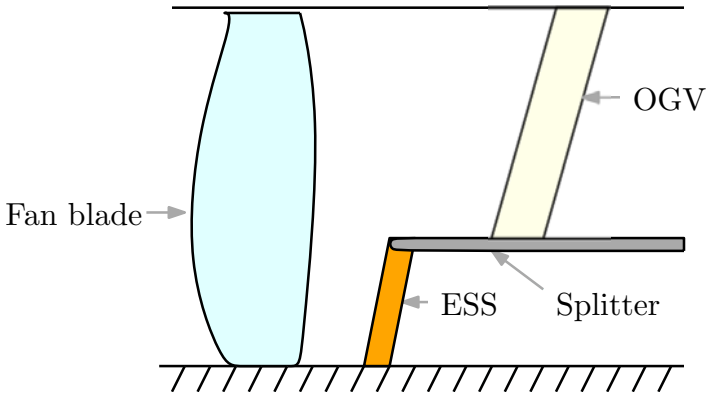

Fig. 2 Illustration of the simplified duct geometry

allows for a 'switch-off' of any of the stator rows in order to evaluate the contributions of OGVs or ESSs separately.

III. Fan Wakes

To determine the unsteady lift fluctuations on the downstream stator row, the incident wake field must be properly defined. This is only possible when the character of the wakes in the velocity field is represented realistically. Many wake models are primarily developed from recorded velocity measurements [6]. A general wake character is then

modelled in an expression that closely matches the measurements at various axial distances from the point of generation. General wake models integrate the drag coefficient, width, and wake centreline velocity deficit, together with the axial direction, into expressions giving the overall velocity deficit in the wake.

The wake models in the prediction method are mainly based on characterization of the centreline velocity deficit and width, and are mostly semi-empirical. For a better representation of modern fans, wake prediction models in references [6, 7] have been included. Geometry and flow effects of the wakes are added as downstream swirl or wake skew [8], and this may significantly alter the harmonic amplitudes when the wake is decomposed into its Fourier components.

The predicted wakes are convected downstream to the stator vanes where the annular wake field at all the leading edges at each radius is calculated. It is notable that the general assumptions for the fan blades may be lifted for the wake prediction, for example, by incorporating wake data directly from CFD calculations or experimental measurements, instead of simpler wake models, thus reflecting the complexity of the wake field.

IV. Predicting the rotor-stator interaction tones

In this section, methods used for the determination of the fluctuating lift on the surfaces of the stators in the downstream blade row, and the in-duct sound power levels, are presented.

A. Upwash, response, loading on vanes and duct acoustics

The response of a downstream cascade of a blade row containing thin airfoils to an incident gust or wake or disturbance has been developed previously, for example, the works by Smith [9] and Whitehead [10]. The two-dimensional approximation avoids the additional complexity introduced when the shape and geometry of a blade are considered. Here, the velocity normal to the chordline of each blade in the cascade is required for the blade response.

The velocity normal to the surface of the reference downstream blade when sweep and lean are considered is found to be

$$\begin{aligned} v_n &= -BU_r \sin(\alpha_1+\alpha_2) \sum_{q=-\infty}^{\infty} \frac{c_1 C_{d_1}}{4\pi r \cos\alpha_1} \exp\left\{ik_Z\left(s_2-\frac{c_2}{2}\right) - ik_{Y_1}(g sin\alpha_1 - l_1)\right\} \\ &\quad \times \exp\left\{-\frac{1}{4\sqrt{\ln 2}}\left[\frac{qb_h B_1}{r\cos\alpha_1}\right]^2 + (i\omega t - ik_Z Z_2 - ik_Y Y_2)\right\} \end{aligned} \tag{1}$$

where B is the number of fan blades, U_r is the relative velocity incident on the fan blade, c_1 and c_2 are the blade and

vane chords, and C_d is the drag coefficient of a fan blade at radius r. The integer q denotes harmonics of the incident upwash, normal to the vane along the chordline. b_h is the wake half-width, and the frequency

$$\omega = \pm qB\Omega\,, \tag{2}$$

for angular velocity Ω of the fan, and wavenumber components

$$k_{Y_1} = \frac{iqB}{r\cos\alpha_1}\sin\alpha_1\,, \tag{3}$$

$$k_Z = \frac{iqB}{r\cos\alpha_1}\sin(\alpha_1+\alpha_2)\,. \tag{4}$$

The implementation of the cascade response methods developed in references [9, 10] for the prediction of interaction tones is clearly presented in references [2, 3], and is not repeated here. Moreover, in order to develop a code to evaluate the acoustic modes in a duct, a number of different boundary conditions are applied to the linear wave equation for particular duct configurations. These boundary conditions ensure the right solution is obtained for that particular duct type. In this case the duct is considered to be a rigid, hard-walled annular duct. The details of the methods for the solution of the wave equation for annular ducts is available in many acoustic texts, for example [11, 12]. The pressure field in an annular duct can be expressed in terms of Fourier–Bessel modes as

$$p(r,\theta,z,t) = \sum_{m=-\infty}^{\infty}\sum_{n=1}^{\infty} P_{mn}^{\pm}\,\psi_{mn}(\kappa_{mn}r)\; e^{i(\omega t - m\theta - k_{z_{mn}}^{\pm} z)}\,. \tag{5}$$

Azimuthal and radial orders are represented by m and n with the corresponding wave numbers $k_{z_{mn}}^{\pm}$ and κ_{mn}, mode shapes ψ_{mn}, and modal amplitudes $P_{mn}^{\pm}$.

B. Green functions

For uniform axial flow in the duct, the inhomogeneous convected wave equation is defined as

$$\left(\frac{\partial^2 p}{\partial t^2} + 2U\frac{\partial p}{\partial x\partial t} + U^2\frac{\partial^2 p}{\partial x^2}\right) - a_0^2\nabla^2 p = \mathcal{F}(\mathbf{x},t)\,, \tag{6}$$

where $\mathcal{F}(\mathbf{x},t)$ is the source distribution, U is the mean axial velocity, and a_0 is the speed of sound. Writing $p = \hat{p}, e^{i\omega t}$, equation (6) reduces to the convected Helmholtz equation. The solution of the inhomogeneous convected Helmholtz

equation for a point source gives the frequency-domain acoustic Green function. For a point source in a rigid, hard-walled duct, the tailored Green function for a point $\mathbf{x} = (r, \theta, z)$ and integration point $\mathbf{x}_0 = (r_0, \theta_0, z_0)$, can be expressed as [3, 11, 12]

$$G(\mathbf{x}|\mathbf{x}_0) = \frac{i}{2A} \sum_{m=-\infty}^{\infty} \sum_{n=1}^{\infty} \frac{\psi_{mn}(\kappa_{mn} r)\psi^*_{mn}(\kappa_{mn} r_0)}{\chi^{\pm}_{mn}} \exp\left\{ ik^{\pm}_{mn}(z - z_0) + \frac{\sqrt{k^2 - \beta^2\kappa^2_{mn}}}{\beta^2}|z - z_0| \right\} \exp\{im(\theta - \theta_0)\} \quad (7)$$

where area $A = \pi(1 - h^2)$ (non-dimensional), $\chi_{mn} = \sqrt{k^2 - \beta^2\kappa^2_{mn}}/\beta^2$ and $k^{\pm}_{mn} = \mp kM + \chi^{\pm}_{mn}$. The pressure field is given by the integration over the blade surface of the product of the blade pressure distribution and a derivative operator acting on the Green function,

$$\hat{p}(\mathbf{x}) = \int_S \nabla G \Delta p_q(\mathbf{x}).\hat{n}\, dS(\mathbf{x}) \,, \quad (8)$$

where S signifies the surface of a vane. Substituting equation (7) into equation (8), after some manipulations and taking integrations in the chordwise and radial directions separately [3, 13], this gives

$$P_{mn} = \frac{\rho_0 V}{2A} \int_h^1 v_q U_r \psi^*_{mn}(\kappa_{mn} r) \left(\frac{m}{r} \cos\alpha_2 + \gamma_{mn} \sin\alpha_2 \right) \times \int_0^{c_2} f_q \exp\left\{ im\theta + \frac{i[kM \pm \sqrt{k^2 - \beta^2\kappa^2}]z}{\beta^2} \right\} dr\, dz \,, \quad (9)$$

where $f_q = \frac{\Delta p_{(q)}}{\rho_0 U_r v_q}$ is the qth harmonic of the Fourier series for Δp. For the qth harmonic, the pressure loading on the jth vane is

$$\Delta p_{j(q)} = \rho_0 v_q U_r f_j e^{-2ijqB/V} \,. \quad (10)$$

Further manipulations as explained in [3] then yields,

$$\frac{P_{mn}}{\frac{1}{2}\rho_0 U^2} = \frac{\sigma_c V}{\pi(1 - h^2)} \int_h^1 \frac{1}{k_{mn}} \left(\frac{U_r}{U}\right)^2 \breve{v}_q \psi_{mn} \left[\frac{m}{r} \cos\alpha_2 + \tilde{\gamma}_{mn} \sin\alpha_2 \right] \tilde{b}\, \aleph_{mn,q} \times \exp\left\{ i[(-\tilde{\gamma}_{mn} x_2)\sigma_c + m y_2/r] - iqB[\sigma_c(y_1 + y_2)/r - z_{o1}\tan\alpha_1 + z_{o1h}\tan\alpha_{1h}] - iqB[\sigma_c \tilde{b}(\sin\alpha_2 + \cos\alpha_2 \tan\alpha_1)/r] \right\} dr \,, \quad (11)$$

where

$$\aleph_{mn,q} = \int_0^{c_2} f_q \exp\left\{ im\theta + \frac{i[kM \pm \sqrt{k^2 - \beta^2\kappa^2}]z}{\beta^2} \right\} dz \,. \tag{12}$$

Green function with Swirl

For the case when the swirl in the interstage is considered, the methods developed in the works by Posson & Peake [14], and further developed by Mathews [15, 16] are used. The acoustic analogy is a rearrangement of the Euler equations into a single linear differential equation for the pressure (represented by the differential operator $\mathcal{F}^{\mathfrak{p}}$), with source term containing the nonlinear and viscosity effects and the rotor-stator geometry. The flow is taken to be inviscid, and is comprised of the base flow and small perturbations, with negligible variations in the radial direction, and can be expressed as

$$(u, v, w) = (U_z(r), 0, U_\theta(r)) \,. \tag{13}$$

For a rigid, hard-walled duct (which is the case considered here), the normal velocity at the wall is zero, which is equivalent to the condition,

$$\frac{\partial p}{\partial r} = 0 \quad r = h \text{ and } r = 1. \tag{14}$$

In Mathews' acoustic analogy [15], the mean pressure, density and speed of sound are

$$\begin{aligned} p(r) &= p(1) - \int_r^1 \frac{\rho_0(r_s) U_\theta^2(r_s)}{r_s} dr_s, \\ \rho_0(r) &= [a_0^2(r)]^{1/\gamma - 1}, \\ a_0^2(r) &= a_0^2(1) + (\gamma - 1) \int_r^1 \frac{U_\theta(r_s)}{r_s} dr_s, \end{aligned} \tag{15}$$

with the base flow in the axial direction $U_z(r)$ and in the circumferential direction $U_\theta(r)$. Modifying the result by Mathews by eliminating the entropy terms, the analogy becomes

$$\mathcal{F}^{\mathfrak{p}}(p) = \mathbb{S}^{\mathfrak{p}} \tag{16}$$

where $\mathcal{F}^{\mathrm{p}}$ is the differential operator given as

$$\mathcal{F}^{\mathrm{p}} = \left(\frac{1}{a_0^2}\frac{D^2}{D_t^2} - \frac{\partial^2}{\partial z^2} - \frac{1}{r^2}\frac{\partial^2}{\partial \theta^2}\right)\mathcal{R}^2 + \left(\frac{1}{r}\frac{D}{D_t} - U_z^{'}\frac{\partial}{\partial z} - \left(\frac{U_\theta}{r^2} + \frac{U_\theta^{'}}{r}\right)\frac{\partial}{\partial \theta}\right)\mathcal{R}\mathcal{T}$$
$$\ldots + \mathcal{R}\frac{D}{D_t}\frac{\partial}{\partial t}\mathcal{T} - \frac{D}{D_t}\left[2U_z^{'}\frac{\partial}{\partial z}\frac{D}{D_t} + 2\left(\frac{U_\theta}{r}\right)^{'}\frac{\partial}{\partial \theta}\frac{D}{D_t} + u_\theta^{'}\right]\mathcal{T} \quad (17)$$

where

$$\frac{D}{D_t} = \frac{\partial}{\partial t} + U_z\frac{\partial}{\partial z} + \frac{U_\theta}{r}\frac{\partial}{\partial \theta}, \quad \mathcal{R} = \frac{D^2}{D_t^2} + U_\theta, \quad \mathcal{T} = \frac{D}{D_t}\frac{\partial}{\partial t} - \frac{2U_\theta}{r^2}\frac{\partial}{\partial \theta} + \frac{U_\theta^2}{r a_0^2}\frac{D}{D_t}, \quad (18)$$

and

$$U_\theta(r) = \frac{2U_\theta(r)}{r}\left(\frac{U_\theta(r)}{r} + U_\theta^{'}(r)\right). \quad (19)$$

The source term $\mathbb{S}^{\mathrm{p}}$

$$\mathbb{S}^{\mathrm{p}} = \mathcal{R}^2(\mathbb{S}_2^{\mathrm{p}}) + \left(\frac{D}{D_t}\left(\frac{1}{r}\frac{\partial}{\partial r}\right) - U_z^{'}\frac{\partial}{\partial z} - \left(\frac{U_\theta}{r^2} + \frac{U_\theta^{'}}{r}\right)\frac{\partial}{\partial \theta}\right)\mathbb{S}_1^{\mathrm{p}} + \frac{D}{D_t}\left[2U_z^{'}\frac{\partial}{\partial z}\frac{D}{D_t} + 2\left(\frac{U_\theta}{r}\right)^{'}\frac{\partial}{\partial \theta}\frac{D}{D_t} + u_\theta^{'}\right]\mathbb{S}_1^{\mathrm{p}}. \quad (20)$$

The pressure can be calculated using a Green function where for the source $\mathbb{S}$, only an approximation of $\mathbb{S}$ is used in the calculation of p. The simplified geometry introduced previously in section II is used. Non-linear terms are ignored, surface terms taken to be insignificant and volume source terms are discarded. The full derivation and expressions for source $\mathbb{S}$ can be found in Matthews' analogy [15].

In order to find the Green function G_ω, the analogy is written in short form as

$$\mathcal{F}^{\mathrm{p}}\left\{G_\omega\right\} = \delta(z - z_0)\frac{\delta(r - r_0)}{r}\delta(\theta - \theta_0)\,. \quad (21)$$

With the entropy a constant, the acoustic analogy is simplified, giving a Green function of the form

$$G_\omega = \frac{1}{4\pi^2}\sum_{m=-\infty}^{\infty} G_m(r|r_0)\, e^{im(\theta-\theta_0)+i\gamma(z-z_0)}\,, \quad (22)$$

where G_n is calculated in the methods explained clearly in references [14–17].

For the particular case of fan-OGV interaction, the focus is on the upstream direction where swirl is considered,

and

$$G_m(r|r_0) = \frac{i}{(2\pi)^2 r_0 C_{mn} D_m(r_0) \Lambda_m^2(r_0) \partial K/\partial\gamma(\gamma_{mn}, r_0)} \psi_{mn}(r)\psi_{mn}(r_0). \tag{23}$$

On non-dimensionalizing by the duct radius r_d, the non-dimensional radius $h \le r \le 1$. Representing the upstream direction by +, the terms in the expression for G_m are given by

$$C_{mn}^{+} = \sigma_r \psi_{mn}^{+}(\sigma_r)\psi_{mn}^{+}(1), \tag{24}$$

$$D_m = \Lambda_m^2 - \frac{2U_\theta}{r_0^2}\frac{d}{dr_0}(r_0 U_\theta), \tag{25}$$

$$\Lambda_m = kU_z + \frac{mU_\theta}{r_0} - \omega, \tag{26}$$

and

$$\partial K/\partial\gamma(\gamma_{mn}^{+}, r_0) = \frac{\rho_0(r_0) D_m(r_0)}{r_0 \rho_0(h) D_m(h)} \left[\frac{\partial^2 \hat{p}_{G,m}}{\partial r_0 \partial\gamma}(\gamma_{mn}^{+}, \sigma_r) + B_{m,k}(h)\frac{\partial \hat{p}_{G,m}}{\partial\gamma}(\gamma_{mn}^{+}, h) - 2\frac{mU_\theta(h)U_z(h)}{h\Lambda_m^2(\sigma_r)}\hat{p}_{G,m}(\gamma_{mn}^{+}, h)\right]. \tag{27}$$

Note that $\hat{p}_{G,m}(r) = \psi_{mn}(r)/\psi_{mn}(1)$ satisfies the boundary condition at the outer wall $r = 1$. The pressure field in an annular duct with swirl is as expressed earlier in equation (5), and for integration over the blade surface with the Green function in an annular duct with swirl, equation (8) yields the modal amplitude for the swirl case as

$$P_{mn} = \sum_{j=1}^{V} e^{2i\pi jm/V} \int_h^1 \int_0^{c_2} S_{mn}^{+}(\omega, r)\Delta p_q = V e^{2i\pi jm/V} \int_h^1 \int_0^{c_2} S_{mn}^{+}(\omega, r)\Delta p_q \, dr\, dz\,, \tag{28}$$

where from [18]

$$S_{mn}^{+}(\omega, r) = \frac{1}{2\pi r C_{mn}^{+} \partial K/\partial\gamma(\gamma_{mn}^{+}, r)} \left\{\left(\frac{m}{r}\cos\alpha_2 + \tilde{\gamma}_{mn}\sin\alpha_2\right)\frac{D_m(r)}{\Lambda_{m,k}(r)}\psi_{mn}(r) - \frac{2\sin\alpha_2 U_\theta(r)}{r\Lambda_m(r)}\left[\frac{d\psi_{mn}(r)}{dr} + B_m(r)\psi_{mn}(r)\right]\right\}, \tag{29}$$

and

$$B_m(r) = \frac{2mU_\theta}{\Lambda_m r^2} - \frac{U_\theta^2}{r a_0^2}\,. \tag{30}$$

In expanded form,

$$\frac{P_{mn}}{\frac{1}{2}\rho_0\overline{U}^2} = \frac{\sigma_c V}{2\pi}\int_h^1 \left(\frac{U_r}{\overline{U}}\right)^2 \breve{v}_q \frac{1}{rC_{mn}\partial K/\partial\tilde{\gamma}_{mn}, r)}$$
$$\left\{\left(\frac{m}{r}\cos\alpha_2 + \tilde{\gamma}_{mn}\sin\alpha_2\right)\frac{D_{m,k}(r)}{\Lambda_{m,k}(r)}\psi_{mn}(r) - \frac{2\sin\alpha_2 U_\theta(r)}{r\Lambda_{m,k}(r)}\left[\frac{d\psi_{mn}(r)}{dr} + B_{m,k}(r)\psi_{mn}(r)\right]\right\}\tilde{b}\aleph_{mn,q}$$
$$\times\exp\left\{i[(-\tilde{\gamma}_{mn}x_2)\sigma_c + my_2/r] - iqB[\sigma_c(y_1+y_2)/r - z_1\tan\alpha_1 + z_{1h}\tan\alpha_{1h}]\right.$$
$$\left. - iqB[\sigma_c\tilde{b}(\sin\alpha_2 + \cos\alpha_2\tan\alpha_1)/r]\right\}dr\ . \quad (31)$$

The two alternative Green functions are implemented in an in-house interaction tone prediction code for both uniform flow and swirl flow in an annular duct. The in-house code, based on the theory outlined in this article, incorporates sections of codes written by Whitehead [4] and Mathews [15, 16] ('GreenSwir'l).

C. Sound Power Level

Having calculated the modal amplitudes P_{mn}, the in-duct modal sound power is

$$P_w = \frac{\pi(r_d^2 - r_h^2)}{\rho_0 U}\sum_{m=-\infty}^{\infty}\sum_{n=1}^{\infty} W_{mn}|P_{mn}|^2\ , \quad (32)$$

where

$$W_{mn} = \frac{\mp M^2\beta^4(qB\Omega/U)k_{mn}}{(qB\Omega/a_0 \pm Mk_{mn})^2}\ , \quad (33)$$

with the upper sign denoting upstream propagating waves, and the lower sign denoting downstream propagating waves. In order to use modal amplitudes of the form in equations (11) and (31), reference [3] suggests non-dimensionalizing by $\frac{1}{8}\rho_0 U^3 M r_d^2$ to give

$$\frac{P_w}{\frac{1}{8}\rho_0 a_0^3 M^4 r_d^2} = \sum_{m=-\infty}^{\infty}\sum_{n=1}^{\infty}\frac{2\pi(r_d^2 - r_h^2)W_{mn}}{Mr_d^2}\left|\frac{P_{mn}}{\frac{1}{2}\rho_0 U^2}\right|^2\ . \quad (34)$$

It is important to note that this formulation for the sound power is only valid in the uniform flow areas - downstream of the OGVs and upstream of the fan.

V. Test Cases and Comparisons

In order to test the output from an in-house code that implements the theory in Sec. IV, a series of test cases are examined. The rotor-stator test case is for 18 rotor blades and 40 stator vanes. A generic geometry is utilised with

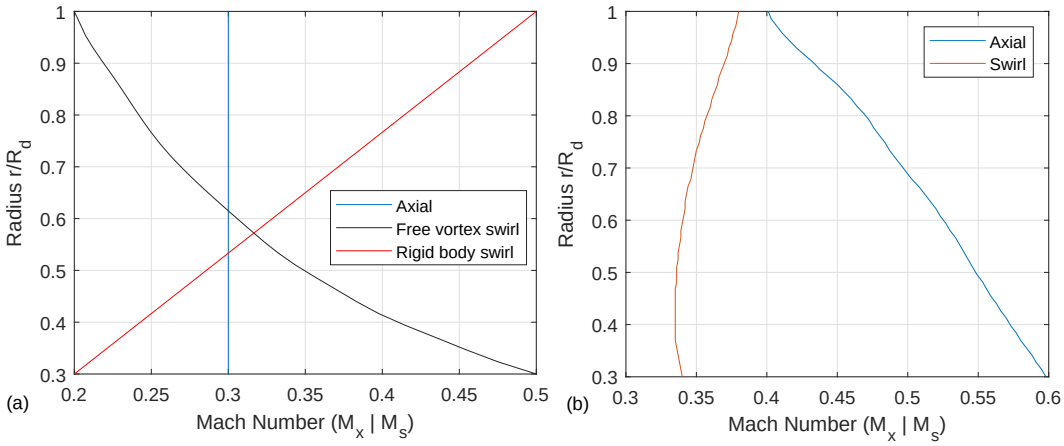

Fig. 3 Test cases: (a) Axial, free vortex and rigid body velocity profiles, (b) Realistic velocity profile.

some variations in the blade sweep, stagger angle, and lean over the radial span. The axial Mach number is set to 0.3 for the uniform flow case, and for the test cases with free vortex swirl or rigid body swirl. An additional calculation is performed for a realistic shear and swirl velocity profile. All the flow profiles are shown in figure 3.

Tables 1 and 2 show the predicted modal amplitudes for the cut-on modes at 2BPF (Blade Passing Frequency) and 3BPF for both the upstream and downstream directions relative to the stator. For this test case, at 1BPF there are no rotor-stator interaction modes that are cut-on. The rotor's rotation speed is set equal to 2,800 revolutions per minute, and the duct radius is equal to 0.5m.

These preliminary test results show how the effect of swirl flow alters the predicted modal amplitudes compared to calculations without swirl flow included. Significantly, some otherwise cut-off modes are cut-on with the inclusion of swirl flow, notably at higher frequencies. At 2BPF, with uniform flow only two radial modes are cut-on for azimuthal order -4, but on introducing either free vortex or rigid body swirl, the third radial mode, (-4,3), is additionally cut-on. This is also observed for the case with the realistic flow profile. At 3BPF, with uniform flow only azimuthal order 14 is cut-on, but with the inclusion of the swirl, additionally azimuthal order -26 is cut-on. However, only one radial order is cut-on for the free vortex swirl, whilst three radial orders are cut-on for the rigid body swirl. Finally, it is noted that at 3BPF, the second radial order of azimuthal order -14 becomes cut-off when the swirl is introduced.

Table 3 shows the number of cut-on modes for predictions with swirl and without swirl (uniform flow), based on an example for a rig-scale engine case. In this case, there are 20 blades and 42 vanes. A fan wake model from reference [2] has been used for the predictions. Subsequent studies will employ the measured wake data. Other information is

Table 1 Upstream Modal amplitudes for test cases with different flow profiles

			Uniform		Free vortex		Rigid body		Realistic	
s	m	n	Modal amplitude		Modal amplitude		Modal amplitude		Modal amplitude	
			real	imag	real	imag	real	imag	real	imag
2	-4	1	-3.2250	1.3640	-0.4967	-0.1018	-0.2391	-0.4384	0.3150	-0.8462
2	-4	2	2.2541	-0.0430	-0.0622	0.7348	-0.6566	0.2121	0.2801	0.9550
2	-4	3	-	-	1.1994	-1.4032	0.3185	1.5569	1.3502	1.1309
3	14	1	-1.0854	-8.1276	-0.0796	-0.0077	0.3297	0.3840	0.0558	-0.0167
3	14	2	0.5277	-2.9618	-	-	-	-	-	-
3	-26	1	-	-	1.0962	0.6239	-0.6145	-0.0228	0.5898	-0.6525
3	-26	2	-	-	-	-	-0.6919	0.6652	0.6711	-0.7189
3	-26	3	-	-	-	-	-0.3929	-2.2175	-	-

Table 2 Downstream Modal amplitudes for test cases with different flow profiles

			Uniform		Free vortex		Rigid body		Realistic	
s	m	n	Modal amplitude		Modal amplitude		Modal amplitude		Modal amplitude	
			real	imag	real	imag	real	imag	real	imag
2	-4	1	3.9147	3.3243	0.0063	-0.0475	0.0422	-0.0423	-0.0407	-0.0294
2	-4	2	-8.7129	0.5936	-0.0237	0.0432	-0.0301	0.0104	0.0594	0.0517
2	-4	3	-	-	0.1979	-0.8420	0.4592	0.2367	0.2611	-0.5125
3	14	1	1.3915	-1.0858	0.5237	0.0747	0.7412	0.5579	-0.4714	-0.2484
3	14	2	1.9314	0.8651	-	-	-	-	-	-
3	-26	1	-	-	0.1034	-0.8819	-0.3048	0.0376	-0.3883	0.2295
3	-26	2	-	-	-	-	-0.2824	0.5545	0.8828	-0.2878
3	-26	3	-	-	-	-	-1.2750	-3.0360	-	-

Table 3 Number of cut-on modes with and without swirl

2BPF			3BPF		
mode	number of radial orders		mode	number of radial orders	
	without swirl	with swirl		without swirl	with swirl
-2	4	4	18	5	4
			-24	4	6

proprietary.

Comparisons of the predicted sound power levels against measured rig-scale engine data are shown in figure 4. The sound power level is shown plotted against the modes that are cut-on at 2BPF and 3BPF, for the upstream (figure 4 (a)) and downstream propagating modes (figure 4 (b)). It is important to note that the power levels are summed over all cut-on radial orders for each azimuthal order. These results are the early development stage outputs generated from the prediction model outlined in this article.

In the upstream direction, at 2BPF the predicted results both have the same number of cut-on radial orders, but comparisons with the measured data shows that the inclusion of swirl significantly reduces the predicted power levels, generally closer to the measured levels. At 3BPF, for the mode 18, the inclusion of swirl also provides an improved prediction compared to the uniform-flow case. The predictions for the -24 mode show larger variability. It is important to point out that the measurements were carried out upstream of the fan, and with acoustic liners installed, whereas the predicted results are for a hard-wall calculation, and the predicted power levels are the interstage levels. Hence, proper comparison can only be done when the fan blockage effects are added to the predictions.

In the downstream direction, comparisons between the measured data and predictions (with swirl) show good agreement at 3BPF for both the 18 and -24 modes. However, at 2BPF the level of the mode -2 is over-predicted when swirl is included, and under-predicted without swirl included.

VI. Conclusion

An overview of the theory for the prediction of Fan-OGV interaction tones with the inclusion of swirling mean-flow has been outlined. Preliminary results for a series of test cases show predictions of the modal amplitudes comparing the results for uniform mean-flow with mean flows that include swirl. The inclusion of the swirl alters the rotor-stator interaction modes that are cut-on. Comparison with measurements show relatively good agreement at higher frequencies especially in the downstream direction where appropriate comparisons can be made.

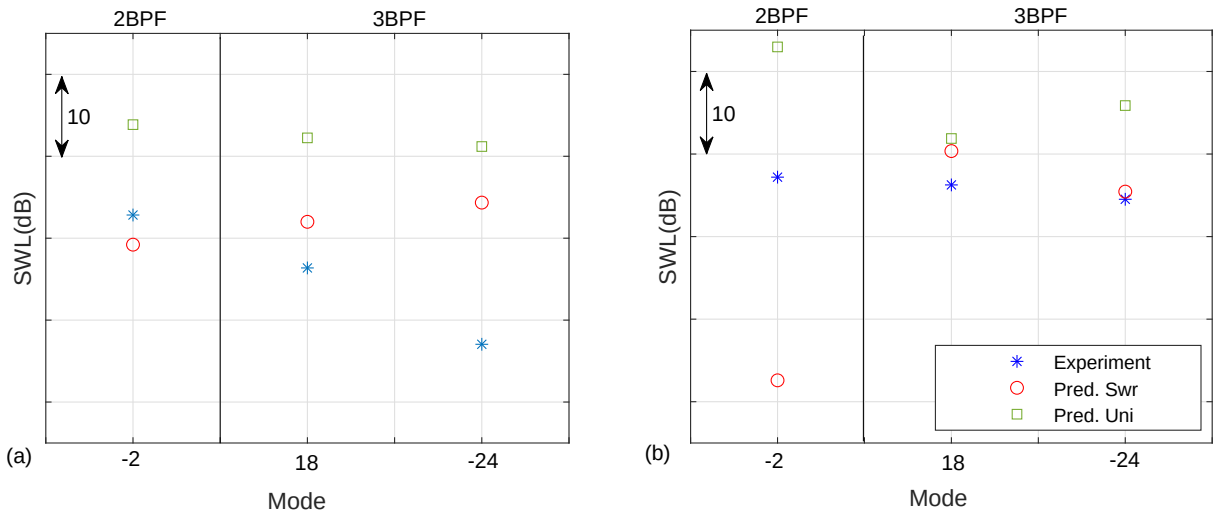

Fig. 4 Sound power level comparisons of experimental measurements against predictions (without swirl [Pred. Uni] and with swirl [Pred. Swr]) (a) Upstream (d) Downstream

Full validation will be carried out to assess the predicted modal powers upstream of the fan (in the inlet duct) and downstream of the stator vanes (in the bypass duct). For upstream propagating sound, it is planned to also include a fan blockage method, to account for the transmission of the inter-stage modes through the rotating fan blades. This study will be presented in a subsequent article.

Acknowledgments

The research was funded by Rolls–Royce plc and Innovate UK in the ACAPELLA and FANTASIA projects. The work was carried out at the Rolls–Royce University Technology Centre in Propulsion Noise Systems (formerly Gas Turbine Noise), Institute of Sound and Vibration Research, University of Southampton.

References

[1] Tyler, J. M., and Sofrin, T. G., "Axial flow compressor noise studies," Tech. rep., SAE Technical Paper, 1962.

[2] Ventres, C., Theobald, M., and Mark, W., "Turbofan noise generation. Volume 1: analysis," *NASA CR–167952*, 1982.

[3] Meyer, H. D., and Envia, E., "Aeroacoustic analysis of turbofan noise generation," *NASA Contractor Report 4715*, 1996.

[4] Whitehead, D., "Classical two-dimensional methods," *In AGARD Aeroelasticity in Axial-Flow Turbomachines.*, Vol. 1, 1987.

[5] Topol, D. A., and Mathews, D. C., "Rotor Wake/Stator Interaction Noise Prediction Code Technical Documentation and User's Manual," *NASA/CR 2010–216818*, 2010.

[6] Majjigi, R., and Gliebe, P. R., *Development of a Rotor Wake/Vortex Model*, National Aeronautics and Space Administration, 1984.

[7] Parry, A. B., "Theoretical prediction of counter-rotating propeller noise," Ph.D. thesis, University of Leeds, 1988.

[8] Brookfield, J., Waitz, I., and Sell, J., "Wake Decay: Effect of Freestream Swirl," *ASME 1997 International Gas Turbine and Aeroengine Congress and Exhibition*, American Society of Mechanical Engineers, 1997.

[9] Smith, S., *Discrete frequency sound generation in axial flow turbomachines*, Citeseer, 1972.

[10] Whitehead, D., *Vibration and sound generation in a cascade of flat plates in subsonic flow*, HM Stationery Office, 1972.

[11] Goldstein, M. E., "Aeroacoustics," *New York, McGraw-Hill International Book Co.*, 1976.

[12] Rienstra, S. W., and Tester, B. J., "An analytic Green's function for a lined circular duct containing uniform mean flow," *Journal of Sound and Vibration*, Vol. 317, No. 3, 2008, pp. 994–1016.

[13] Clark, T., Ganz, U., Graf, G., and Westall, J., "Analytic Models of Ducted Turbomachinery Tone Noise Sources," *NASA CR-132443, May*, 1974.

[14] Posson, H., and Peake, N., "The acoustic analogy in an annular duct with swirling mean flow," *Journal of Fluid Mechanics*, Vol. 726, 2013, pp. 439–475.

[15] Mathews, J., *Mathematical modelling of noise generation in and propagation through turbomachinery*, PhD Thesis, University of Cambridge, 2016.

[16] Mathews, J. R., Peake, N., and Bianchi, S., "Asymptotic and numerical Green's functions in a lined duct with realistic shear and swirl," *22nd AIAA/CEAS Aeroacoustics Conference*, 2016, p. 2922.

[17] Bender, C. M., and Orszag, S. A., *Advanced mathematical methods for scientists and engineers I: Asymptotic methods and perturbation theory*, Springer Science & Business Media, 2013.

[18] Masson, V., Posson, H., Sanjose, M., Léonard, T., Moreau, S., and Roger, M., "Fan-OGV interaction broadband noise prediction in a rigid annular duct with swirling and sheared mean flow," *22nd AIAA/CEAS Aeroacoustics Conference*, 2016, p. 2944.